# An Improved Approach of Quantifying Magnetic Moments of Small *in-vivo* Objects

**C-Y. Hsieh[1], Y-C. N. Cheng[1], J. Neelavalli[1], and E. M. Haacke[1]**

[1]Wayne State University, Detroit, Mi, United States

**Introduction:** It is a challenge to quantify the susceptibilities of small *in-vivo* objects such as veins. During the past three years, we have developed a complex sum method that can be used to determine the susceptibility of cylinders with small radii from MR images (see Eq. 1) [1, 2]. Our previous studies of the complex sum method [2, 3] required the knowledge of the object size. In this abstract, we present an improved approach to solve the magnetic moment without any a prior information of the cylindrical object size or its susceptibility. After finding the magnetic moment of the cylindrical object, the susceptibility and size of the object may be solved numerically. In addition, we have studied uncertainties of this method through simulations.

**Simulations and Methods:** We simulated an image with a long cylindrical air tube perpendicular to the main field and inserted in the middle of a gel phantom, as it was acquired with TE=5 ms from the 1.5T MR scanner [2]. The radius of the tube (a) and image resolution are 1 mm. The susceptibility of the gel was assumed to be -9 ppm in SI unit so the effective magnetic moment *p*, defined as the product of the susceptibility and the square of the tube radius, is 9.03 ppm·mm$^2$. An example set of magnitude and phase images are shown in Fig. 1. The black dot at the center of the magnitude image in Fig. 1 represents the cross section of the tube. From Eq. 1 and sum of complex MR signals $S_i$ within each of the three circles (with radii $R_1$, $R_2$, and $R_3$) shown in Fig. 1, the magnetic moment *p* becomes the only unknown variable in Eq. 2. Because each $p/R_i^2$ in Eq. 2 is the maximum phase value at the boundary of the *i*-th circle, with each circle chosen to be larger than the area where phase aliases, each $p/R_i^2$ can be guaranteed to be less than one radian. This condition ensures Eq.2 can be numerically solved with only one solution. The uncertainties of *p* can be studied through error propagation of Eq. 2.

**Results:** The complex sums from both the simulated MR image and theoretical results are reproduced in Table 1 [2]. Using the complex sum results from three circles, the effective moment *p* is solved in Table 2. Most of these results are accurate within 10% of the theoretical value. This fact demonstrates the feasibility of this improved method. In this abstract, we only study the uncertainty due to the discretization effect in MR images. Table 3 lists the differences of complex sum signals used in Eq. 2 and their comparisons to the associated analytical results as shown in Eq. 3. These numbers are necessary for the study of the discretization uncertainty through the error propagation method. The error propagation method with numbers in Table 3 indicates that the results of uncertainties are consistent with those listed in Table 2.

**Discussions:** It is possible to minimize the discretization uncertainty by properly choosing the radii of the three circles from a given MR image. With ($R_1$/a,$R_2$/a,$R_3$/a) = (3,4,5) and the calculated effective magnetic moment *p* = 9.03 ppm·mm$^2$, one may want to choose circles with maximum phase values at each circle in the phase image are close to 1, 1/2, and 1/3, respectively. Alternatively, we have found that with the choice of maximum phase values of 0.9, 0.6 and 0.3 for the three circles, ($R_1$/a, $R_2$/a, $R_3$/a) = (3.2,3.9,5.5), respectively, the effective magnetic moment can become -8.93 ppm·mm$^2$. This result leads to less than 1% uncertainty. In summary, we have shown that the improved method is feasible of extracting the magnetic moment of a small object within good accuracy.

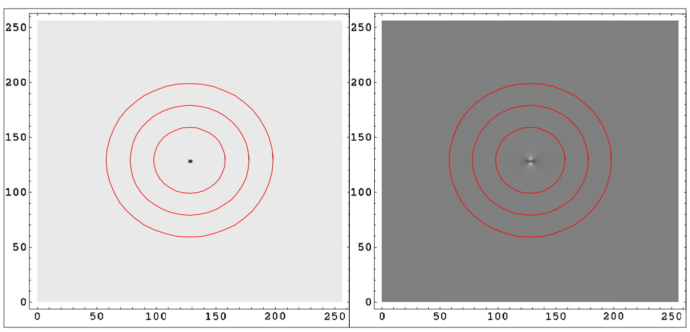


Fig.1 Simulated MR magnitude (left) and phase (right) images (256x256)

$$S_i = \pi l \rho_0 p \int_{p/R_i^2}^{g} dx \frac{J_0(x)}{x^2} ----------------(1)$$

$$(S_1 - S_2)\times \int_{p/R_2^2}^{p/R_3^2} dx \frac{J_0(x)}{x^2} = (S_2 - S_3)\times \int_{p/R_1^2}^{p/R_2^2} dx \frac{J_0(x)}{x^2} ----(2)$$

$$S_i - S_j = A_i - A_j + \Delta(AS)_{ij} -------------(3)$$

where the effective magnetic moment $p \equiv g\, a^2$. ($g \equiv 0.5\, \gamma\, B_0\, \Delta\chi$ TE and $\Delta\chi$ is magnetic susceptibility), a is the tube radius, $J_0$ is the Bessel function, and $\rho_0$ is the spin density but contains the imaging parameters.

Table 1: Complex signal with discretization uncertainty only

| Radius ratio $R_i$/a | Analytical $A_i$ | Simulation $S_i$ |
|---|---|---|
| 3 | 6.96 | 7.51 |
| 4 | 25.96 | 26.21 |
| 5 | 52.81 | 52.82 |
| 6 | 86.59 | 86.46 |
| 7 | 126.96 | 126.79 |

**References**: [1] Cheng et al., ISMRM, p. 1719, 2004

[2] Hsieh et al., Medical Physics, p. 1910, 2005

[3] Hsieh et al., ISMRM, p.1836, 2006

Table 2: Magnetic moment *p* solved from three circles

| $R_1$/a | $R_2$/a | $R_3$/a | *p* | *p*(%) |
|---|---|---|---|---|
| 3 | 4 | 5 | -9.33 | 3.3 |
| 3 | 4 | 6 | -9.39 | 4.0 |
| 3 | 4 | 7 | -9.43 | 4.4 |
| 4 | 5 | 6 | -9.76 | 8.1 |
| 4 | 5 | 7 | -9.84 | 9.0 |
| 5 | 6 | 7 | -10.21 | 13.1 |

Table 3: Differences of complex sum between simulations and theoretical results

| $R_i$/a | $R_j$/a | ΔAij | ΔSij | $\Delta(AS)_{ij}$ | Error% |
|---|---|---|---|---|---|
| 3 | 4 | 19 | 18.7 | 0.3 | 1.6 |
| 3 | 5 | 45.85 | 45.31 | 0.54 | 1.2 |
| 3 | 6 | 79.63 | 78.95 | 0.68 | 0.8 |
| 3 | 7 | 120.00 | 119.28 | 0.72 | 0.6 |
| 4 | 5 | 26.85 | 26.61 | 0.24 | 0.9 |
| 4 | 6 | 60.63 | 60.25 | 0.38 | 0.6 |
| 4 | 7 | 101 | 100.58 | 0.42 | 0.4 |
| 5 | 6 | 33.78 | 33.64 | 0.14 | 0.4 |
| 5 | 7 | 74.15 | 73.97 | 0.18 | 0.2 |
| 6 | 7 | 40.37 | 40.33 | 0.04 | 0.1 |